Plastic Flow Instability in 304 Austenitic Stainless Steels at Room Temperature

J. TABIN, K. NALEPKA, J. KAWAŁKO, A. BRODECKI, P. BAŁA, and Z. KOWALEWSKI

A remarkable plastic flow instability is observed during tensile deformation of the commercial 304 stainless-steel sheet at room temperature. It has been found that the occurrence of plastic flow instability in 304 is dependent on the strain rate and specimen gage length. Moreover, it is essentially the same as the necking caused by plastic instability in 316L. However, the enhanced strain hardening resulting from deformation-induced martensitic transformation facilitates the orderly propagation of the strain-localized band.

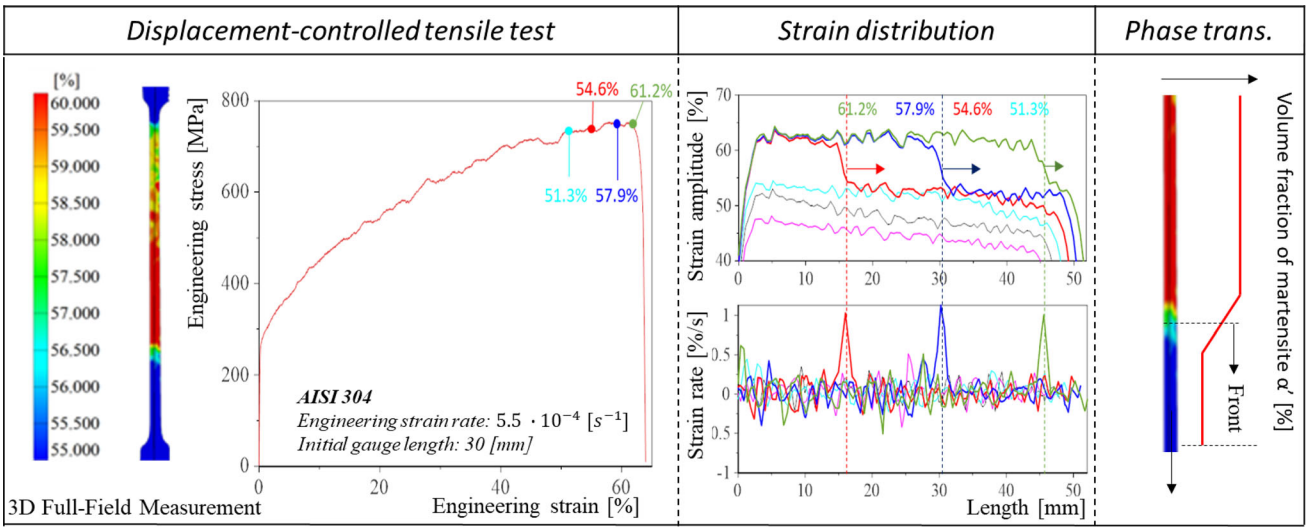

https://doi.org/10.1007/s11661-023-07223-5

AUSTENITIC stainless steels (ASS) of AISI 304 and AISI 316L grades are characterized by very good mechanical properties and corrosion resistance over a wide range of temperatures. As a result, they find numerous applications in the automotive, aviation, nuclear, and chemical industries, as well as in space and superconducting technology, where temperature changes occur from room temperature to even absolute zero.[1,2] The temperature below which plastic deformation can induce the martensitic transformation (M_d) in ASS is usually above room temperature. However, it depends on the chemical composition. It is reduced by alloying elements, *i.e.*, Cr and Ni, as they stabilize austenite. Similar effect is provided by N, Mn, and Mo. M_d for the studied ASS 304 is about 50 °C.[3] As the temperature decreases, below the threshold M_d, the volume fraction of martensite generated by the same strains increases. The coupling between temperature

J. TABIN, A. BRODECKI, and Z. KOWALEWSKI are with the Institute of Fundamental Technological Research, Polish Academy of Sciences, 02-106 Warsaw, Poland. Contact e-mail: jtabin@ippt.pan.pl K. NALEPKA is with the Faculty of Mechanical Engineering and Robotics, AGH University of Science and Technology, 30-059 Kraków, Poland. J. KAWAŁKO and P. BAŁA are with the Academic Centre for Materials and Nanotechnology, AGH University of Science and Technology, 30-059 Kraków, Poland.

Manuscript submitted July 10, 2023; accepted October 1, 2023.

Published online: 18 October 2023

(main driving force for the phase transformation) and deformation is shown by another quantity, M_{d30}. It constitutes the temperature at which 30 pct true strains produce 50 pct volume content of martensite. Angel[4] developed a useful formula for M_{d30} as a function of chemical composition. According to this formula, M_{d30} for the tested ASS 304 and 316L is approximately 16 °C and − 22 °C, respectively. It is well known that, in addition to the chemical composition of ASS,[5] the rate of martensite formation is highly dependent on factors such as, deformation temperature[4,6] and strain rate.[7,8] Martensite formation is responsible for enhancing the work hardening rate, increasing uniform elongation, or inhibiting necking.[7] This phenomenon is known as the transformation-induced plasticity (TRIP).[5,7] The TRIP effect in 304 metastable austenitic steels during tension is often mentioned in the literature,[8–11] but it is never clearly defined: Is there a strain threshold at which the TRIP effect initiates? How does the TRIP effect correlate with the strain rate of loading? Alternatively, does it depend on the geometry of the specimen?

The present study aims to clarify the mechanism of stable propagation of strain-localized bands in commercial 304 stainless-steel sheets during displacement-controlled tension at room temperature. The results are presented in the context of the findings obtained for 316L. The impact of the test parameters is identified, including strain rate and gage length limits. The basis for this investigation is *in situ* tensile tests conducted at room temperature and recorded using Digital Image Correlation (DIC). By analyzing the deformation fields and identifying the accompanying stable propagation of the strain-localized band at different test parameters, we aim to gain a better understanding of the underlying mechanism.

Commercial sheets of 304 and 316L austenitic stainless steels, with a thickness of 1 mm, are used in the present study. The chemical composition of the 304 steel is C-0.07 pct, Cr-18 pct, Ni-10 pct, Mn-2 pct, and Si-0.8 pct. The 316L steel had a composition of C-0.03 pct, Cr-18.2 pct, Ni-11.5 pct, Mn-2 pct, Mo-2 pct, and Si-1.0. The dog bone-shaped tensile test specimens are fabricated using electrical discharge machining (EDM) from commercial stainless-steel sheets (304 and 316L) with the tensile axis aligned with the rolling direction. The semi-products are supplied in the annealed and lightly cold-rolled conditions (304 and 316L) according to the standards ASTM A480 and EN 10088. In these forms, the materials are typically used for structural components that operate over a wide range of temperatures.[2] The initial microstructure [Figure 1(b)] of the as-received materials in all cases consists of equiaxed, fully recrystallized grains with recrystallization twins present in some of the larger grains. The average grain size is comparable in the 304 and 316L steels, measuring 15.6 and 19.2 μm, respectively.

To analyze the structural behavior of specimens and the deformation mechanism of austenitic stainless steels, the Digital Image Correlation (DIC) technique is employed during the displacement-controlled tensile tests [see Figure 1(a)]. The strain distribution during tension is monitored using DIC Aramis 12 M, equipped with lenses having a total focal length of 75 mm and calibrated settings suitable for the measuring area of 170 × 156 mm or 38 × 25 mm. Calibration is performed prior to testing using a certified GOM calibration plate. In this study, the results of the DIC analysis are presented in the form of strain amplitude and strain rate distributions along the specimen axis for different traverse displacements [see Figures 1(a) and 2].

The displacement-controlled uniaxial tensile tests are conducted on dog bone specimens of 304 and 316L stainless steel at room temperature, with a crosshead velocity of 1 mm/min and 10 mm/min. The supplementary material contains MP4 files from the tensile tests of 304 (Movie 1). During the tests, the strain distribution is continuously monitored to analyze the strain amplitude and strain rate along the specimen axis. In the initial stage of tension [Figures 2(b) and (c)], a uniform distribution of strain is observed in both the 304 and 316L specimens (bottom strain amplitude curves). However, as tension continued, necking occurred in the 316L, while a visible front formed in the 304 specimen (red curve). The strain-localized band propagated along the specimen, starting from the bottom and moving towards the upper grip. Interestingly, different modes of front propagation are also observed. For instance, the two strain-localized bands started from opposite sides of the specimen (see Figure 5).

The front propagation in 304 is attributed to the accumulation of strain rate within a narrow band. Although it exhibits similarities to necking caused by plastic instability in 316L, the enhanced strain hardening promotes the stable propagation of the localized strain band, thereby increasing the ductility of the metastable specimen (known as the TRIP effect). ASS 304 steel has a less favorable chemical composition compared to 316L steel, resulting in a lower stacking fault energy and making it more susceptible to the TRIP effect. Therefore, at the tested strain levels, we observe the TRIP effect only in 304 steel. A similar effect was reported by Abu-Fahra *et al.*,[12] who studied a high-strength steel containing 10 pct Mn with a two-phase austenite and ferrite microstructure. In their case, the austenite was enriched in C and Mn, which lowered the stacking fault energy. When combined with a considerable fraction of ferrite, this resulted in a relatively high local strain in austenite grains at the early stages of deformation, leading to the activation of the TRIP effect with Lüders-type plastic front propagation. Thus, it is well known that chemical composition influences the plastic flows instability in ASS, but how do test parameters influence it?

To investigate the impact of test parameters, the tests are conducted at different crosshead velocities: 1 mm/min and 10 mm/min (engineering strain rates $\dot{\varepsilon}$: 5.5×10^{-4} s^{-1} and $5.5 \times 10^{-3} s^{-1}$). The results are presented in Figure 3. It is observed that for the test conducted at 1 mm/min ($\dot{\varepsilon} = 5.5 \times 10^{-4}$ s^{-1}), the

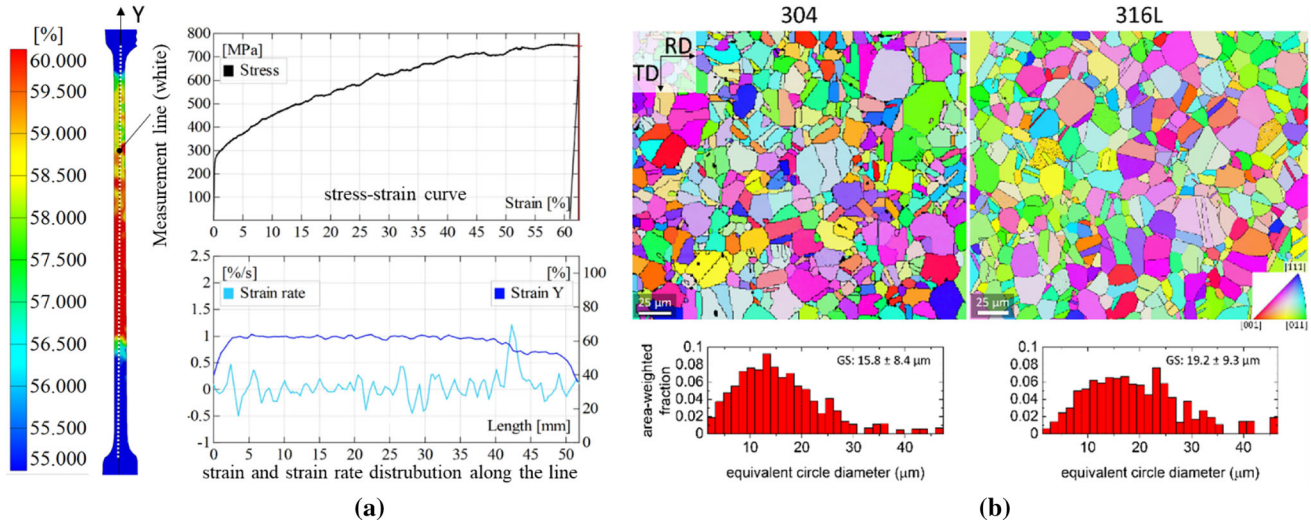

Fig. 1—(*a*) Digital Imaging Correlation system for strain distribution analysis along the vertical (*Y*) line. Stress–strain curve and strain and strain rate distribution along the line (software: GOM Correlate 2019). (*b*) The microstructures of the investigated materials, as received, are shown in the top row as inverse pole figure (IPF) maps. IPF coloring relative to the ND axis. The bottom row displays the grain size distributions in terms of equivalent circle diameter (Color figure online).

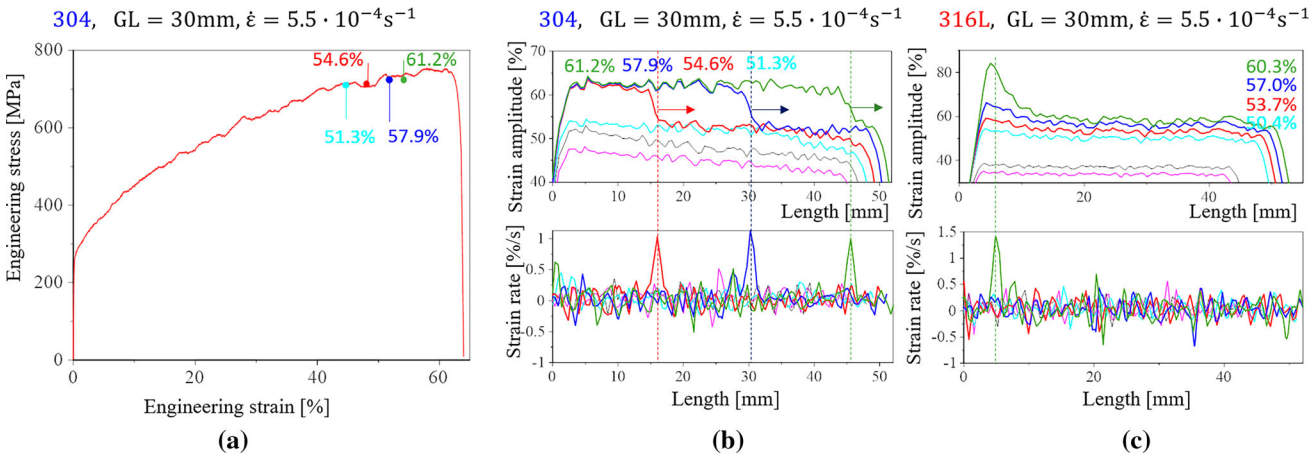

Fig. 2—Results of displacement-controlled tension (engineering strain rate: $\dot{\varepsilon} = 5.5 \times 10^{-4}s^{-1}$) of 304 and 316L dog bone specimens (gage length: GL = 30 mm) at room temperature; (*a*) engineering stress–engineering strain curve for 304; (*b*) and (*c*) strain amplitude along the line for different engineering strains, based on it the strain rate is calculated. (b) Front propagation in 304 is indicated by arrows (Color figure online).

strain-localized band exhibits stable propagation, followed by necking and rupture. The front propagation is associated with the accumulation of strain rate within a narrow band. Conversely, for tests conducted at velocities higher than 10 mm/min ($\dot{\varepsilon} = 5.5 \times 10^{-3}$ s^{-1}), the plastic flow instability in the 304 specimen is essentially the same as necking caused by plastic instability in the 316L specimen.

The plastic flow behavior is influenced by the gage length of the specimen. The displacement-controlled tensile tests of 304 are conducted at a crosshead velocity of 1 mm/min ($\dot{\varepsilon} = 5.5 \times 10^{-4}$ s^{-1}). The results are presented in Figure 4. For gage lengths greater than 26 mm, the stable propagation of the strain-localized band is observed, followed by necking and rupture. Similar to previous observations, the front propagation is associated with the accumulation of strain rate within a narrow band. On the other hand, for specimens with gage lengths lower than 24 mm, the plastic flow instability in the 304 specimen is essentially the same as necking caused by plastic instability, similar to what is observed in the 316L specimen.

It is worth noting that the critical length of the parallel part of the dog bone specimen has been identified for the 304 specimens at room temperature. Additionally, to capture the plastic flow instability in 316L, the test is carried out using a dog bone specimen with a gage length of 40 mm [Figure 4(c)]. In this case, the front propagation is still not observed, and after uniform deformation, necking occurs.

To clarify the mechanism of the stable propagation of the strain-localized band in 304, the distribution of martensitic content along the line is measured during test by means of feritscope Mp3C. It is a device designed

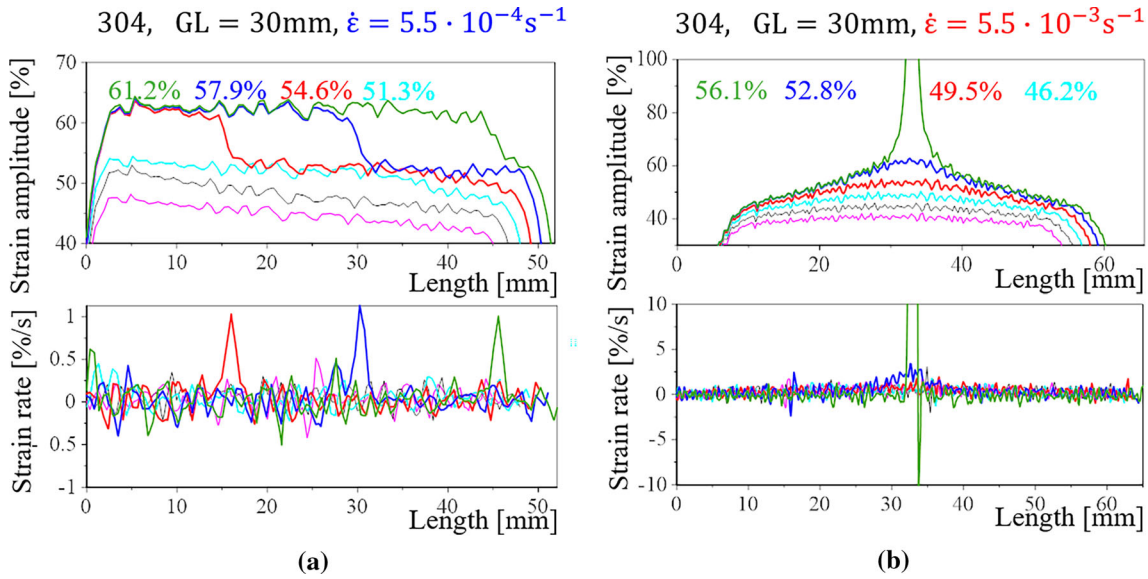

Fig. 3—Strain rate effect on the propagation of the strain-localized band in 304 dog bone specimens (GL = 30 mm). Strain amplitude along the line and strain rate for two crosshead velocities: (*a*) 1 mm/min ($\dot{\varepsilon} = 5.5 \times 10^{-4}s^{-1}$) and (*b*) 10 mm/min ($\dot{\varepsilon} = 5.5 \times 10^{-3}s^{-1}$).

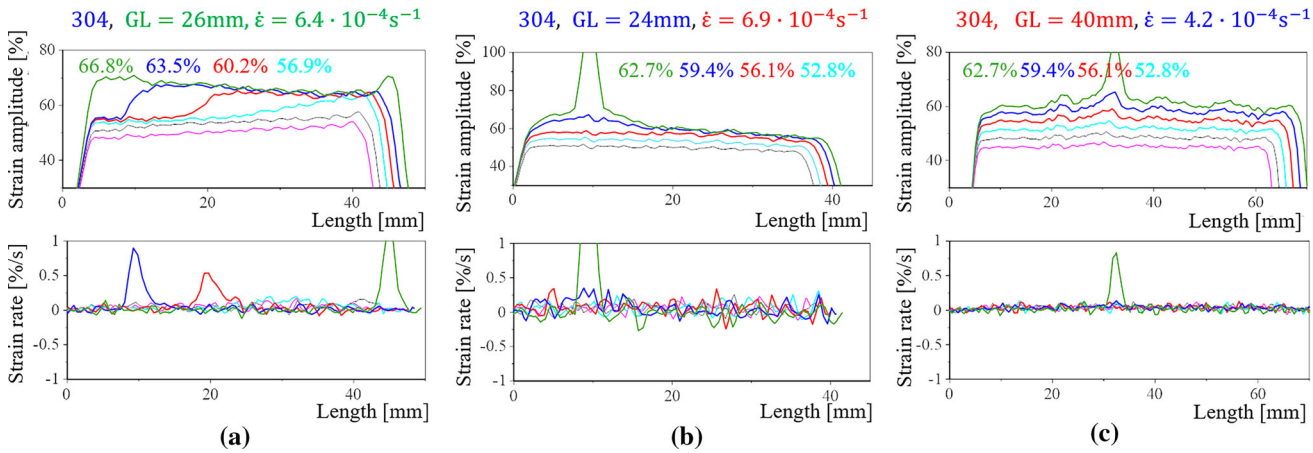

Fig. 4—Gage length effect on the propagation of the strain-localized band in 304 and 316L dog bone specimens. Strain amplitude along the line and engineering strain rate $\dot{\varepsilon}$ for different gage lengths GL: (*a*) 24 mm, (*b*) 26 mm, and (*c*) 40 mm.

for ferrite content measurements, but after calibration can be also used to measure the volume fraction of martensite α' in ASS.[13,14] The measurement of new phase distribution along the specimen axis is performed during a displacement-controlled, loading-unloading tension test at room temperature. In order to avoid the Villari effect (inverse magneto-strictive effect),[15] the martensite content is measured after unloading, at specific points, along the specimen axis. The results are presented in Figure 5. Thus, during the initial stage of deformation, uniform strain as well as martensite content distributions are observed (green curves). As the total strain increases, heterogeneity of strain and martensite α' occurs, particularly when front propagation is observed [Figure 5(b)]. The feritscope measurement reveals that the area behind the front has a higher volume fraction of martensite α' (magenta curve). After exceeding 54 pct of the local strain (see Figure 5), there is a rapid production of the secondary phase. Referring to the works of Murr *et al.*,[3] the observed effect results from the avalanche-like joining of properly densely distributed embryos of martensite α'. The continuation of tension induces the transfer of localized deformation with the associated rapid growth of the secondary phase. Thus, the plastic flow instability in the 304 material is essentially the same as necking caused by plastic instability in 316L, but the stable propagation of the strain-localized band is realized through enhanced strain hardening by deformation-induced martensitic transformation, leading to the large ductility of the material. It is worth pointing out that such an effect is observed in ultra-fine-grained austenitic stainless steel,[16] nevertheless the strain rate and geometry effects have not been addressed yet. The experimental results show that at higher traverse velocity (10 mm/min), the front propagation is not observed in 304. The strain and secondary phase maintain a uniform distribution [*cf.* Figures 5(b) and (c)].

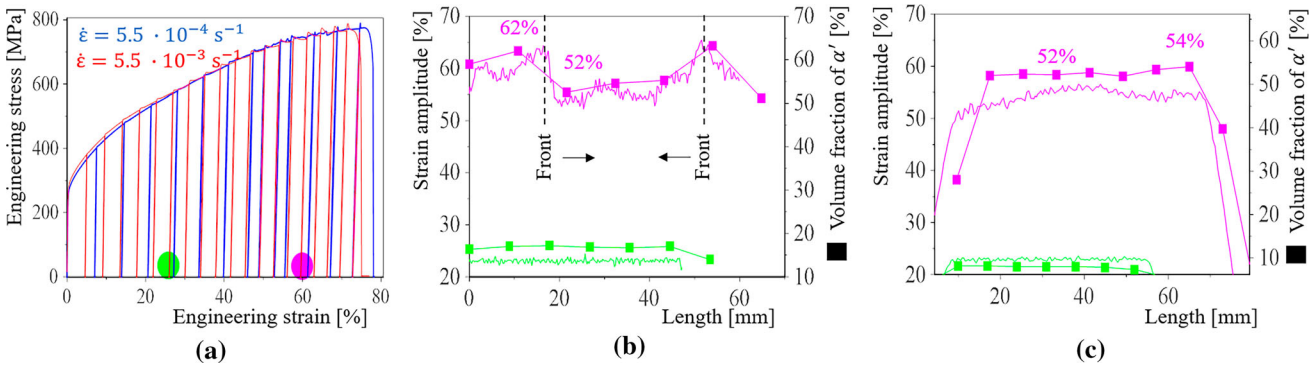

Fig. 5—(*a*) Stress–strain curves of displacement-controlled, loading-unloading test of 304 at room temperatures, GL = 30 mm (blue: 1 mm/min, $\dot{\varepsilon} = 5.5 \times 10^{-4}\text{s}^{-1}$ and red: 10 mm/min, $\dot{\varepsilon} = 5.5 \times 10^{-3}\text{s}^{-1}$); (*b*) and (*c*) volume fraction of martensite α' (squares) *vs* strain amplitude along the specimen axis measured after unloading cycles (for green and magenta dot, respectively). (b) Stable propagation of the strain-localized band is observed for strain rate $\dot{\varepsilon} = 5.5 \times 10^{-4}\text{s}^{-1}$ (arrows); (c) Uniform distribution of strain amplitude and volume fraction of martensite α' is observed for strain rate $\dot{\varepsilon} = 5.5 \times 10^{-3}\text{s}^{-1}$ (Color figure online).

The following question arises: Does locally high strain rate within the plastic instability promote a more complete TRIP? The presented experimental results make it possible to provide an answer. The front propagation manifests by accumulated strain rate [Figure 4(a)]. It generates a greater number of intersecting shear bands and, thus, embryos of martensite α', which leads to their faster coalescence and enhances TRIP effect.[3] The test results show that a global increase in strain rate (ten times) eliminates beneficial local hardening of the material. This is due to the more intensified formation of martensite α' nuclei evenly distributed along the gage length [Figure 5(c)]. This arrangement likely makes it difficult to concentrate the phase transformation in the natural notches present in the specimen. Consequently, the local weaknesses are not sufficiently strengthened, and front propagation is not observed [Figure 3(b)]. Moreover, as the specimen slenderness decreases, the uniaxial stress state is replaced by a complex state. As a result, a non-uniform strain distribution is formed, which concentrates the phase transformation in an area other than the initial notches present in the sample. The research, combining DIC and feritscope measurements, demonstrates for the first time that, with the metastable material (304) and test conditions, a plastic strain front propagating can be activated at room temperature. As a result, the locally arising TRIP effect improves ductility. We believe that the presented results shed new light on the complex phenomena observed during plastic deformation of commercially available ASS 304 sheet. However, further investigations regarding adiabatic heating,[17] static or dynamic strain aging[18,19] or microstructural evolution during the plastic deformation of ASS, particularly over a wide range of temperatures, are required.

SUPPLEMENTARY INFORMATION

The online version contains supplementary material available at https://doi.org/10.1007/s11661-023-07223-5.

ACKNOWLEDGMENTS

This work has been supported by the National Science Centre through the Grant No. 2019/35/B/ST8/03151. The authors would like to express their gratitude to the M. Wyszkowski and D. Kukla for technical support.

CONFLICT OF INTEREST

On behalf of all authors, the corresponding author states that there is no conflict of interest.

REFERENCES

1. F. Bertinelli, F. Fudanoki, T. Komori, G. Peiro, and L. Rossi: *IEEE Trans. Appl. Supercond.*, 2006, vol. 16, pp. 1773–76.
2. P. Fernández-Pisón, J.A. Rodríguez-Martínez, E. García-Tabarés, I. Avilés-Santillana, and S. Sgobba: *Eng. Fract. Mech.*, 2021, vol. 258, p. 108042.
3. L.E. Murr, K.P. Staudhammer, and S.S. Hecker: *Metall. Trans. A*, 1982, vol. 13A, pp. 627–35.
4. T.H. Angel: *J. Iron Steel Inst.*, 1954, vol. 177(5), pp. 165–74.
5. M.J. Sohrabi, M. Naghizadeh, and H. Mirzadeh: *Arch. Civ. Mech. Eng.*, 2020, vol. 20, p. 124.
6. J. Tabin: *Mech. Mater.*, 2021, vol. 163, p. 104090.

7. B.C. De Cooman: *Curr. Opin. Solid State Mater. Sci.*, 2004, vol. 8, pp. 285–303.
8. J. Talonen: Ph.D. Thesis, 2007, p. 127.
9. S.S. Hecker, M.G. Stout, K.P. Staudhammer, and J.L. Smith: *Metall. Trans. A*, 1982, vol. 13A, pp. 619–26.
10. W. Bleck, X. Guo, and Y. Ma: *Steel Res. Int.*, 2017, vol. 88, p. 1700218.
11. N. Tsuchida, E. Ishimaru, and M. Kawa: *ISIJ Int.*, 2021, vol. 61, pp. 556–63.
12. F. Abu-Farha, Hu. Xiaohua, X. Sun, Y. Ren, L.G. Hector, G. Thomas, and T.W. Brown: *Metall. Mater. Trans. A*, 2018, vol. 49A, pp. 2583–96.
13. J. Talonen, P. Aspegren, and H. Hänninen: *Mater. Sci. Technol.*, 2004, vol. 20, pp. 1506–12.
14. R. Ortwein, B. Skoczeń, and J. Ph Tock: *Int. J. Plast.*, 2014, vol. 59, pp. 152–79.
15. B. Cao, T. Iwamoto, and P.P. Bhattacharjee: *Mater. Sci. Eng. A*, 2020, vol. 774, p. 138927.
16. Yu. Si Gao, R.Z. Bai, Y. Tian, W. Mao, A. Shibata, and N. Tsuji: *Scripta Mater.*, 2019, vol. 159, pp. 28–32.
17. C.B. Finfrock, D. Bhattacharya, B.N.L. McBride, T.J. Ballard, A.J. Clarke, and K.D. Clarke: *JOM*, 2022, vol. 74, pp. 506–12.
18. M. Thrun, C. Finfrock, A. Clarke, and K. Clarke: *Front. Mater.*, 2021, vol. 7, pp. 1–6.
19. J. Mola, G. Luan, Q. Huang, C. Ullrich, O. Volkova, and Y. Estrin: *Acta Mater.*, 2021, vol. 212, p. 116888.